Spark Plasma Sintering of Nanocrystalline Cu and Cu-10 Wt Pct Pb Alloy

AMIT S. SHARMA, KRISHANU BISWAS, BIKRAMJIT BASU, and DIBYENDU CHAKRAVARTY

For the first time, we report here that high purity nanocrystalline Cu and Cu-10 wt pct Pb alloys can be densified with more than 90 pct theoretical density at a low temperature of 623 K (350 °C) using spark plasma sintering (SPS) in argon atmosphere at a pressure of 100 MPa. Scanning electron microscopy (SEM) analysis indicates that molten Pb particles travel through Cu grain boundaries, delineating a "flowlike" pattern in the microstructure. An extensive transmission electron microscopy (TEM) analysis of the ultrafine scale microstructure reveals partial wetting of Cu by liquid Pb as well as entrapment of Pb particles within the Cu matrix. The sintering kinetics and microstructural evolution are discussed in reference to the intrinsic characteristics of SPS as well as phase equilibria in the Cu-Pb system. An important result is that high hardness of around 2 GPa is measured in the Cu-10 wt pct Pb nanostructured alloy, SPS at 573 K to 623 K (300 °C to 350 °C).

DOI: 10.1007/s11661-010-0589-4
© The Minerals, Metals & Materials Society and ASM International 2010

I. INTRODUCTION

ALLOYS of Cu-Pb have been used extensively in various engineering applications, because of their superior friction and wear properties as compared to other materials, such as aluminum-bronze, copper-beryllium, and Babbitt alloys. These bulk alloys have been traditionally fabricated by the casting route.[1,2] However, immiscibility of Pb in Cu leads to compositional inhomogeneity due to segregation in the interdendritic regions during the casting process, leading to poor tribological properties.[3] Added to this, the casting process leads to large scale pore formation, degrading the mechanical properties of the bulk components.[1,2] On the other hand, homogenous distribution of second phase and controlled porosity for self-lubricating bearings can be obtained in the sintered alloys. Das and Upadhyaya[4] showed that, for the case of microcrystalline Cu with 12 wt pct Pb, pressureless sintering at 1173 K (900 °C) is necessarily required to obtain 80 pct theoretical density. A major limitation to achieve a superior tribological property of the sintered alloy is the low hardness of the matrix and inhomogeneous distribution of the second phase in the microstructure.[4] This is mainly attributed to micron-sized grains of the Cu matrix. It will be possible to achieve high hardness using nanocrystalline Cu grains, where intrinsically higher hardness due to finer grains as well defect structure would improve the tribological property.

However, the primary challenge for the material scientists in manufacturing bulk nanostructured materials is to retain the intrinsic nanometric size of the constituent phases in the sintered bulk component. From the thermodynamics perspective, nanocrystalline constituents have to be thought of as bulk grains with a significant fraction of grain boundaries.[5,6] The grain boundaries, being nonequilibrium entities, provide a larger driving force for grain coarsening during sintering, owing to their mobility.[5,6]

In the present work, we have made an attempt to synthesize the bulk nanostructured Cu-10 wt pct Pb hypo-monotectic alloy by a novel technique, spark plasma sintering (SPS), using elemental powder mixtures. The selection of alloy composition is made to strike a balance between the mechanical properties (*e.g.*, hardness) and densification enhancement due to Pb addition. It is expected that pure Cu would exhibit solid-state sintering, while SPS above 600 K (327 °C) would melt Pb, leading to liquid phase sintering (LPS) of the Cu-Pb compact. Using the advantages of SPS, *i.e.*, shorter holding time and lower processing temperatures, tailoring SPS parameters to densify nanostructured Cu-Pb bulk components with optimum density will be demonstrated. It is reported that highly localized temperature and subsequent spark discharge between powder particles would activate particle surfaces by the removal of the oxide film.[7] During the SPS process, the holding pressure, holding time, and current/voltage pulse play an important role in the process. In view of this, both the pressure and temperature are independently varied in the present work to obtain high density Cu and Cu-Pb alloy with nanosized grains.

AMIT S. SHARMA, Research Scholar, KRISHANU BISWAS, and BIKRAMJIT BASU, Associate Professors, are with the Department of Materials and Metallurgical Engineering, Indian Institute of Technology, Kanpur 208016, UP, India. Contact e-mail: kbiswas@iitk.ac.in DIBYENDU CHAKRAVARTY, Scientist C, is with the International Advanced Research Centre for Powder Metallurgy and New Materials, Balapur PO, Hyderabad 500005, AP, India.
Manuscript submitted June 20, 2010.
Article published online January 5, 2011

Apart from SPS parameters optimization, this article reports the microstructural development in the Cu-Pb alloy. An understanding of phase equilibria in the Cu-Pb system is necessary to analyze the microstructure of alloys, spark plasma sintered at different temperatures. The phase diagram for the Cu-Pb system is shown in Figure 1.[8] The Cu and Pb form a typical monotectic alloy system having a miscibility gap between 36 and 87 wt pct Pb, being virtually immiscible with each other at low temperatures. A monotectic reaction occurs at 36 wt pct Pb at 1228 K (955 °C) involving liquid 1, liquid 2, and almost pure Cu:

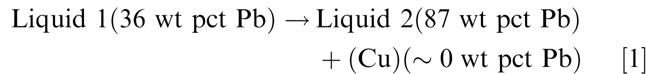

$$\text{Liquid 1(36 wt pct Pb)} \rightarrow \text{Liquid 2(87 wt pct Pb)} + \text{(Cu)}(\sim 0 \text{ wt pct Pb}) \quad [1]$$

According to the equilibrium diagram (Figure 1), highly Pb-rich liquid 2 solidifies at lower temperature of ~599 K (326 °C) to Cu plus Pb *via* the following eutectic reaction:

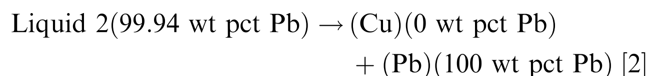

$$\text{Liquid 2(99.94 wt pct Pb)} \rightarrow \text{(Cu)(0 wt pct Pb)} + \text{(Pb)(100 wt pct Pb)} \quad [2]$$

One of the objectives of the present work is to show how the microstructure development and phase assemblage in SPS samples is characteristically different from the one predicted from the equilibrium phase diagram.

II. EXPERIMENTAL DETAILS

A. *Sample Preparation*

High purity commercial nanocrystalline Cu powder (mean particle size ~97 nm, 99.8 pct purity, Sigma-Aldrich, St. Louis, MO) and microcrystalline Pb powder (mean particle size ~149 μm, 99.98 pct purity, Sigma-Aldrich) were used as the starting materials. The starting powder mixture consisting of Cu with 10 wt pct

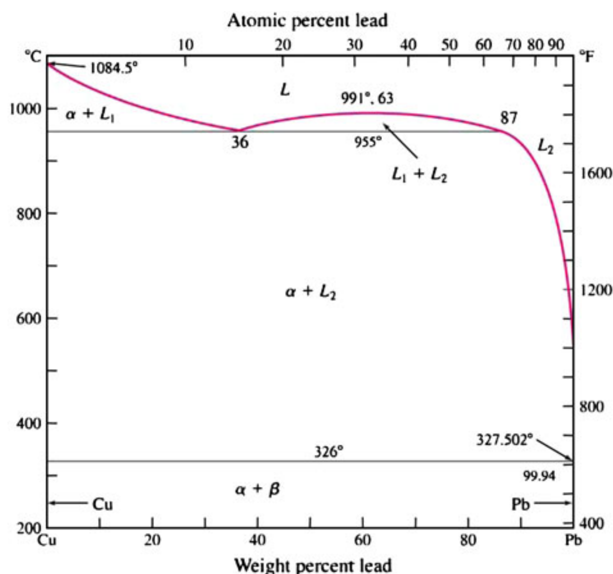

Fig. 1—Equilibrium Cu-Pb binary phase diagram.[8]

Pb was ball milled for 16 hours using tungsten carbide (WC) balls in a WC vial with acetone as the grinding media at 200 rpm. The low energy milling operation of the premixed powders was performed in a planetary micromill (Fritsch Pulverisette 7, Idar-Oberstein, Germany). The acetone level in the vial was monitored in such a way that the powder mixture was completely immersed in the grinding media throughout the milling operation. The powder slurry was then filtered and dried in an oven at about 353 K (80 °C) to obtain a homogenously mixed powder. Similarly, pure nanocrystalline Cu powder was ball milled for 16 hours to obtain agglomerate-free powder for sintering. SPS was carried out using a Dr. Sinter 515S apparatus (SPS Syntex Inc., Kanagawa, Japan) with a pulse on-off ratio of 12:2. The powder mixture, loaded in a graphite die of 15-mm diameter, was placed inside the SPS chamber between two graphite electrodes under a vacuum of 6 Pa. High purity argon was then purged with a flow rate 2 L/min in the chamber to ensure minimal oxidation of the powders. The powder was heated with the heating rate of 80 K/min to the sintering temperature and held at the sintering temperature for 5 minutes before it was furnace cooled to room temperature. The sintering temperature used in the present study ranged from 523 K to 873 K (250 °C to 600 °C). The temperature of the sample was monitored using a K1-type chromel-alumel thermocouple, which was inserted in the die at a distance of 13 mm from the inner die wall so that the recorded temperature difference between the sample and die was minimum. A uniaxial pressure of 100 MPa was applied throughout the sintering cycle. The real time data of the variation of voltage, current, temperature, pressure, and displacement of punches were recorded during each SPS run and for all samples. During the SPS experiment, while a constant voltage of 20 V was applied, the current flow varied around 1500 A. The final height of the spark plasma sintered samples varied between 1 and 2 mm. In order to obtain complementary information on sintering induced shrinkage, dilatometry experiments were carried out on green compacts of both Cu and Cu-10 wt pct Pb in the temperature range of RT to 873 K (600 °C) in argon atmosphere. The heating rate employed was 5 K/min.

B. *Characterization*

The density of all SPS processed samples was determined according to Archimedes' principle using distilled water. The theoretical density for the sintered composition was calculated following the rule of mixtures, considering the theoretical densities of pure Cu and Pb as 8.94 and 11.92 gm/cc, respectively. The phase identification of the polished and flat samples was performed by X-ray diffraction (XRD) (Seifert, Ahrensburg, Germany) using Cu K_α (λ = 0.154056 nm) radiation at a scan rate of 0.5 deg/min. For microstructural characterization, the samples were ground and polished using 5- and 1-μm alumina slurry as polishing media to remove the external surfaces and to produce optically reflecting metallographic surfaces. The phase distribution of all the polished samples was observed using a field emission scanning electron microscope

(FEI Sirion, Hillsboro, OR and Carl Zeiss Supra 40 VP, GmbH, Oberkochen, Germany), operated at 20 kV. Transmission electron microscopy (TEM) observations were carried out using a 200 kV (FEI Technai, 20UT) microscope. Sample preparation for TEM observations involved mechanical thinning of 3-mm discs, followed by ion milling to electron transparency in a Gatan 691 precision ion polishing system. The ion polishing was carried out using a beam energy of 4 keV and incident angle of 4 deg to minimize heating and sample damage. The sample was ion milled at 2 keV and 2 deg incident angle to clean the sample surface from contamination. Vickers hardness of the sintered samples was measured using a Vickers microhardness tester (Bareiss Prüfgerätebau, GmbH) by applying 200-g load. In order to obtain reliable measurement of hardness, the diagonals of Vickers indents were measured using an optical microscope. Pore size distributions of the green compacts were obtained using the Barrett, Joyner, and Halenda method from adsorption-desorption isotherms at 77 K (–196 °C) (Micromeritics ASAP 2020, Norcross, GA).

III. RESULTS

A. *Densification of the Composite*

Figure 2 shows the variation of relative density with temperature for nanocrystalline Cu-10 wt pct Pb alloy and pure nanocrystalline Cu sintered at 100 MPa. Overall, the variation of sinter density with SPS temperature follows a similar trend for both nanocrystalline Cu-10 wt pct Pb and nanocrystalline Cu; *i.e.*, sinter density goes through a maximum with SPS temperature. For pure nanocrystalline Cu, the maximum densification is achieved at 673 K (400 °C) (~87 pct ρ_{th}), whereas nanocrystalline Cu-10 wt pct Pb can be sintered to density of ~ 90 pct ρ_{th} at 623 K (350 °C). This reveals that with 10 wt pct Pb addition, the SPS temperature required to obtain comparable density is around 323 K (50 °C) lower than pure Cu. The density of nanocrystalline Cu-10 wt pct Pb decreases as the sintering temperature increases further up to 873 K (600 °C). However, for pure nanocrystalline Cu, density decreases very little as the sintering temperature increases from 673 K to 873 K (400 °C to 600 °C). It is clear from Figure 2 that the addition of 10 wt pct Pb assists in attaining comparatively higher density at lower SPS temperature *vis-à-vis* nanocrystalline Cu. In order to assess the progress of densification with temperature, the instantaneous relative density, defined as $(\rho_{instantaneous}/\rho_{theoretical}) \times 100$ pct, is plotted in Figure 3. The instantaneous density is computed on the basis of real time dilatometer measurements during an SPS run. For SPS experiments in the temperature region of 573 K to 673 K (300 °C to 400 °C), the increase in instantaneous density shows comparable values and an almost similar trend. However, the densification is largely restricted at higher SPS temperature of 873 K (600 °C), and a maximum of 75 pct ρ_{th} is obtained in the sintered compact. On the basis of the results presented in Figures 2 and 3, the following can be summarized.

(a) It is important to optimize the SPS temperature in a narrow window to obtain higher attainable density in the Cu-Pb system.
(b) It is possible to obtain 90 pct ρ_{th} in nanocrystalline Cu-10 wt pct Pb alloy at 623 K (350 °C).
(c) Degradation of density occurs in the temperature window of 623 K to 873 K (350 °C to 600 °C).

B. *Phase Analysis by XRD*

Figure 4 shows the XRD patterns acquired from polished surfaces of Cu and Cu-10 wt pct Pb samples, sintered at different sintering temperatures. The dotted lines at the bottom show the characteristic peaks of different phases per the ICDD database. The characteristic peaks of both Cu and Pb are marked in Figure 4. The diffractogram (Figure 4(a)) corresponding to pure nanocrystalline copper shows a substantial presence of

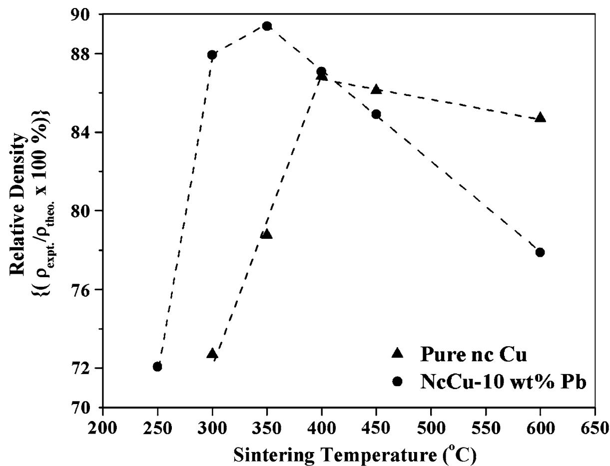

Fig. 2—Relative density of sintered samples using SPS as a function of sintering temperature at a pressure of 100 MPa.

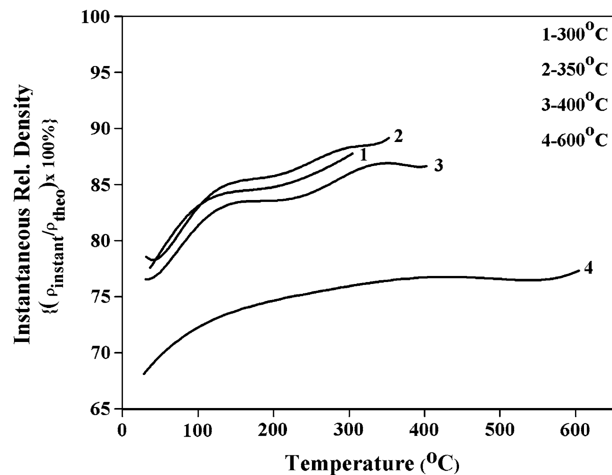

Fig. 3—Variation of instantaneous relative density $[(\rho_{instant}/\rho_{theo}) \times 100$ pct] with temperature of Cu-10 wt pct Pb, SPS at 100 MPa.

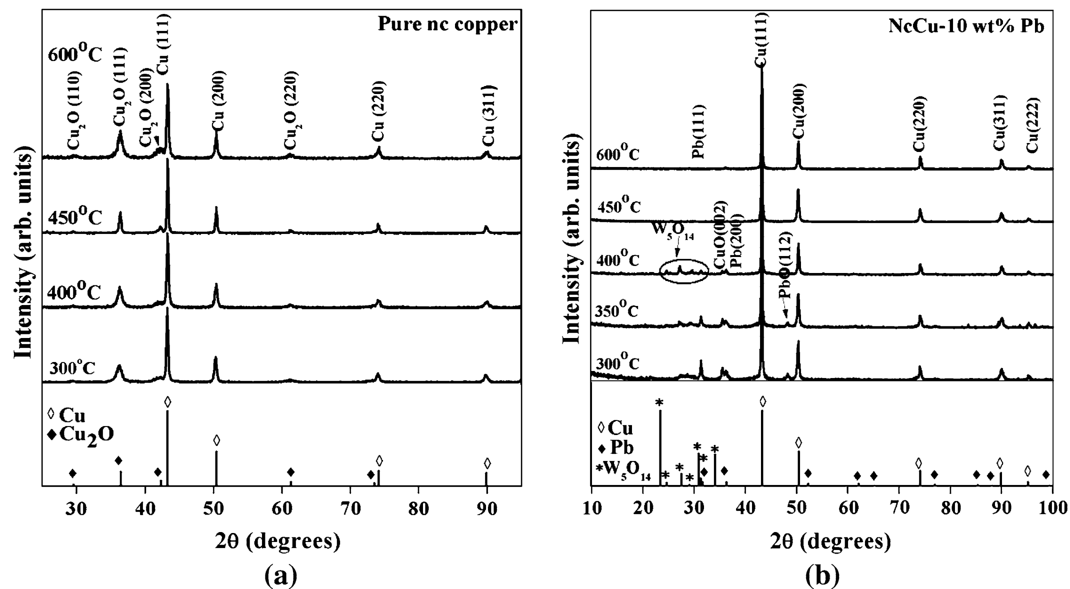

Fig. 4—XRD patterns of (*a*) pure Cu and (*b*) Cu-10 wt pct Pb, SPS at 100 MPa.

Cu_2O. The oxidation of copper is supposed to have an adverse effect on the effective density obtained in the Cu compact compared to the Cu-10 wt pct Pb composite. On the other hand, nanocrystalline Cu-10 wt pct Pb samples show characteristic Cu and Pb peaks at lower sintering temperatures of 573 K, 623 K, and 673 K (300 °C, 350 °C, and 400 °C) (Figure 4(b)). However, as the sintering temperature is raised beyond 673 K (400 °C), the intensity of the (111) peak of Pb is too weak to be detected. Also, the characteristic Cu_2O peaks, which are present in the case of pure nanocrystalline Cu, are absent in the case of nanocrystalline Cu-10 wt pct Pb. The nanocrystalline Cu-10 wt pct Pb, sintered compact, spark plasma sintered at 673 K (400 °C), exhibits some peaks corresponding to the tungsten-oxide (W_5O_{14}). The presence of W_5O_{14} may be related to the contamination of powder mixture in the course of the ball-milling process.

C. *Microstructural Characterization*

Scanning electron microscopy (SEM) analyses of Cu-10 wt pct Pb, sintered at different temperatures, are shown in Figure 5. Figure 5(a) is a representative backscattered electron (BSE) micrograph of a sample sintered at 573 K (300 °C). The presence of Cu grain boundaries could not be deciphered in the BSE micrograph. However, it depicts uniform distribution of Pb throughout the Cu matrix. The inset of Figure 5(a) shows Pb particles of 1- to 2-μm size. The isolated porosity is distinctly visible (marked by black arrows) in the micrograph. As the temperature is raised to 623 K (350 °C), Pb particles (Figure 5(b)) are found to be resolidified during cooling from the sintering temperature. One can observe that the molten Pb particles have traveled through the Cu grain boundaries, delineating a "flowlike" pattern of Pb in the microstructure. It is difficult to discuss here more on particle morphology or grain sizes, which are later discussed on the basis of the analysis of TEM images. The inset of Figure 5(b) illustrates the formation of multiple fragmented Pb particles. One can also observe the presence of cracks in the Pb particle. Further at 723 K (450 °C), Pb has formed well-interconnected contours, distributed throughout the matrix (Figure 5(c)). The inset of Figure 5(c) shows smaller Pb fragments with diffuse boundaries. Noteworthy here also is the appearance of isolated porosity and some smaller ones in a quite continuous manner, prevailing throughout the microstructure. At higher temperature of 873 K (600 °C) (Figure 5(d)), Pb morphology in the matrix is distinctly different from that of low-temperature sintered samples. At 873 K (600 °C), Pb particles appear in small globules, which are well dispersed throughout the matrix. The interfacial energy variation with temperature at the Cu-Pb interface is responsible for the Pb particle assuming the geometrically isotropic shape.

Some important results from the TEM analysis are shown in Figures 6 through 9. Figure 6(a) presents a representative bright-field micrograph of the sample, sintered at 573 K (300 °C), revealing fine scale Cu grains. The elongated Pb particles are marked by yellow arrows on Figure 6(a). A large number of bright-field micrographs are used to obtain grain size distribution of Cu grains. Figure 6(c) shows the grain size distribution indicating that the mean grain size is 82 ± 39 nm. The detailed microstructural characterization reveals the presence of a large number of grains with nanoscale twins. Figure 6(b) illustrates one such grain with nanoscale twins. A representative bright-field micrograph of the sample sintered at 623 K (350 °C) is shown in Figure 7(a). The Pb particles are marked by yellow arrows on the micrograph. The presence of nanosized Pb particles inside the Cu grains was observed and confirmed by the EDS technique. The observation of distinct Pb phase in the vicinity of Cu grain boundaries

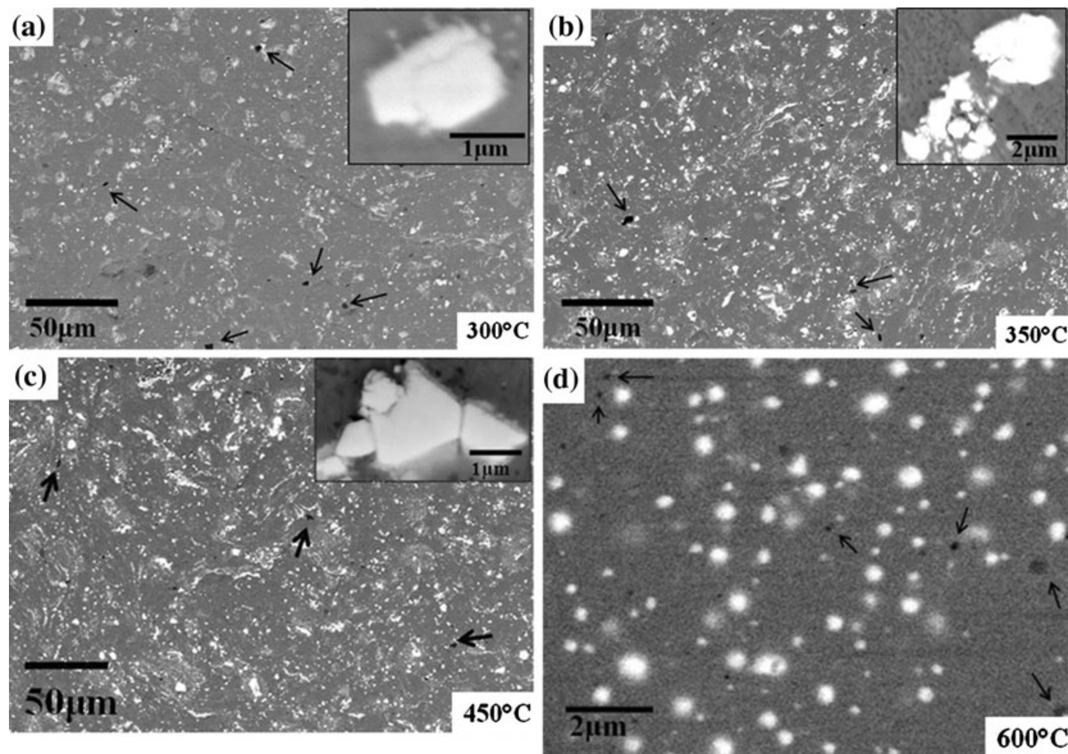

Fig. 5—BSE SEM micrographs of Cu-10 wt pct Pb samples SPS at various temperatures: (*a*) 573 K (300 °C), (*b*) 623 K (350 °C), (*c*) 723 K (450 °C), and (*d*) 873 K (600 °C). Black arrows mark the pores.

is consistent with the immiscibility of Cu and Pb at 623 K (350 °C). However, the encapsulated Pb particle in the vicinity of the triple junction at the GB region of Cu grains has been the most characteristic morphology of Pb (Figure 7(b)). It is also revealed that some of the Cu grains are deformed significantly during sintering. The presence of a large number of dislocations inside Cu grains is good evidence of deformation (inset of Figure 7(a)). The measured grain-size distribution (Figure 7(c)) shows a skewed characteristic, with the maximum percentage of grains being less than 100 nm. The size distribution also exhibits the largest fraction in the 50- to 100-nm size range with a mean grain size of 124 ± 68 nm.

Figure 8(a) shows a typical bright-field micrograph of the alloy samples, sintered at 673 K (400 °C), revealing substantial growth of Cu grains. The grain-size distribution depicts that, though a larger fraction of grains are in the 110- to 190-nm range, a considerable fraction has grown beyond 200 nm, with the largest population in the 200- to 250-nm size range (Figure 8(b)). The mean grain size is 199 ± 88 nm. Some of the Cu grains showed anisotropic growth, as indicated in Figure 8(a). The arrows mark the Pb particles on the micrograph. The inset of Figure 8(a) reveals one such elongated grain. These grains might have some molten Pb in their vicinity and have attained elongated morphology with deformed structure in their interior. Such observation is consistent with the characteristic microstructure, observed in any liquid phase sintered material.

Figure 9 shows a typical bright-field micrograph of the sample, sintered at 873 K (600 °C). The Cu grains have been found to grow significantly in excess of 500 nm. The grain size distribution, as obtained from TEM micrographs, is shown in Figure 9(c). It can be clearly observed that a large number of the grains (approximately 2/3 of total number of Cu grains) have grown to 1 to 2 μm. The Pb particles have been found both at the triple junction of Cu grains and inside the Cu grains. Figure 9(b) reveals the dark-field TEM image of a typical Cu grain showing a well-developed dislocation network. This reflects a large scale deformation, experienced by the Cu matrix during SPS densification at 100 MPa pressure.

D. *Hardness Measurements*

Figure 10 shows the hardness variation of the pure nanocrystalline Cu and nanocrystalline Cu-10 wt pct Pb samples sintered at 100 MPa and at different temperatures. At least five measurements were carried out for each sample. The average value is reported with error bars, indicating the standard deviation. The samples sintered at low sintering temperatures (573 K and 623 K (300 °C and 350 °C)) show very high hardness (~2 GPa) as compared to the samples sintered at 723 K to 873 K (450 °C to 600 °C) (~0.8 GPa). In the present study, the load applied was 200 g, and so there will not be any indentation size effect.[9] Srivatsan *et al.*[10] reported the hardness variation of the bulk

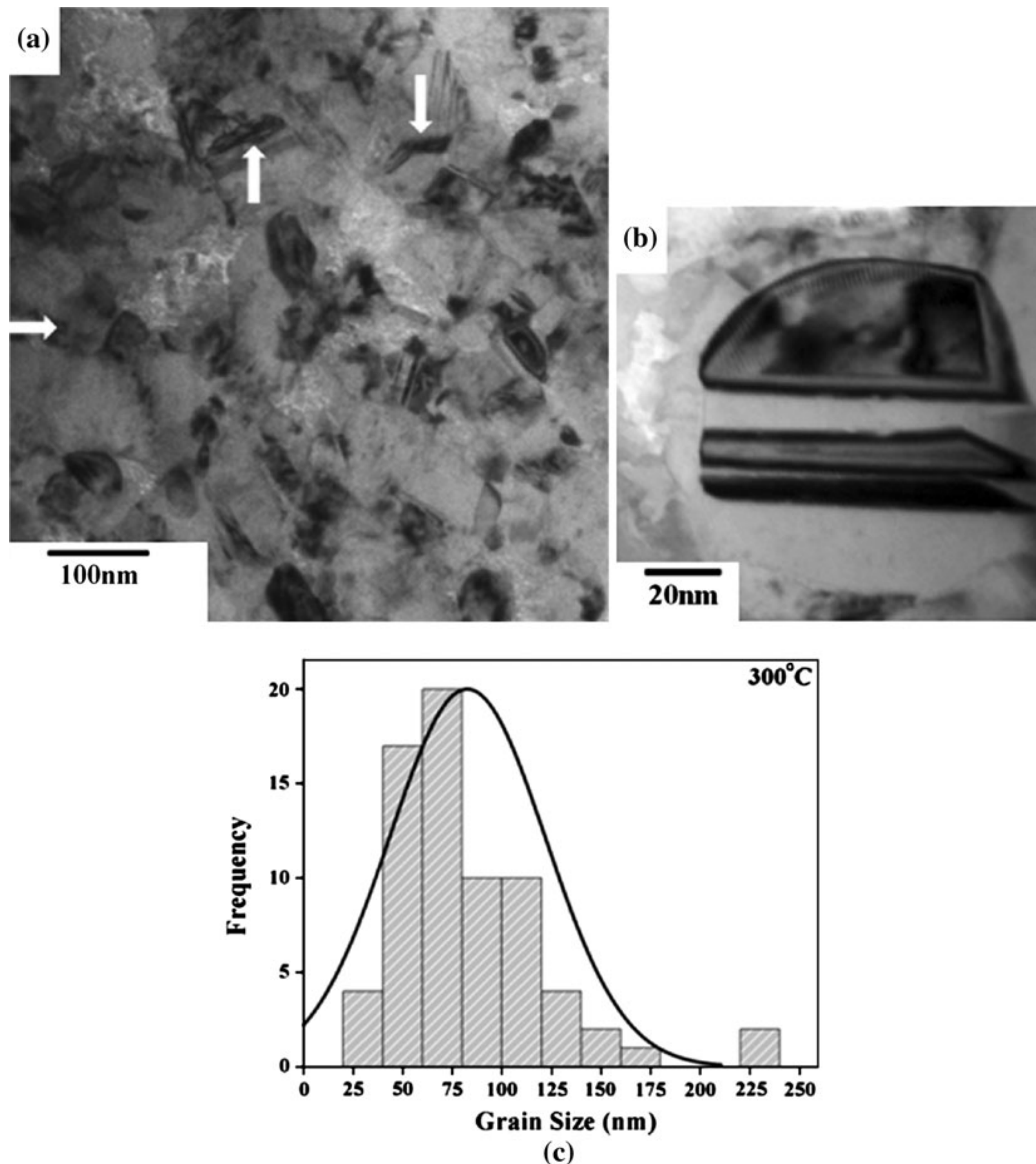

Fig. 6—(*a*) Bright-field micrograph of Cu-10 wt pct Pb sample processed at sintering temperature of 573 K (300 °C) and 100 MPa. (*b*) Grain showing nanotwin formation and (*c*) Cu grain-size distribution. Arrows mark the Pb position in the matrix.

Cu samples prepared by the plasma pressure compaction technique. The average reported values of microhardness and nanohardness were 1.9 and 2.4 GPa, respectively, after sintering at 1153 K (880 °C) with 50 MPa pressure. The attainment of high bulk hardness of 2 GPa in nanocrystalline Cu-10 wt pct Pb alloy, in the present study, therefore, indicates that 10 wt pct Pb addition (soft phase) does not significantly degrade the hardness property.

IV. DISCUSSION

The present investigation has clearly demonstrated that it has been possible to densify nanocrystalline Cu and Cu-10 wt pct Pb alloys and retain nanometer sized matrix grains by SPS. The sintering temperature has been reduced from 723 K to 1073 K (450 °C to 800 °C) to 573 K to 673 K (300 °C to 400 °C) because of the addition of Pb in nanocrystalline Cu as compared to pure microcrystalline Cu.[4–11] In addition to lowering of the sintering temperature, a holding time of only 5 minutes is required for SPS in contrast to the couple of hours needed for pressureless sintering.[4–10] Therefore, Pb can be effectively used as the sinter additive for achieving better and faster densification during SPS. This is considered to be a major improvement as far as the bulk processing of nanocrystalline Cu-Pb composite is concerned. The microstructural analysis using SEM and TEM indicates the homogeneous distribution of Pb

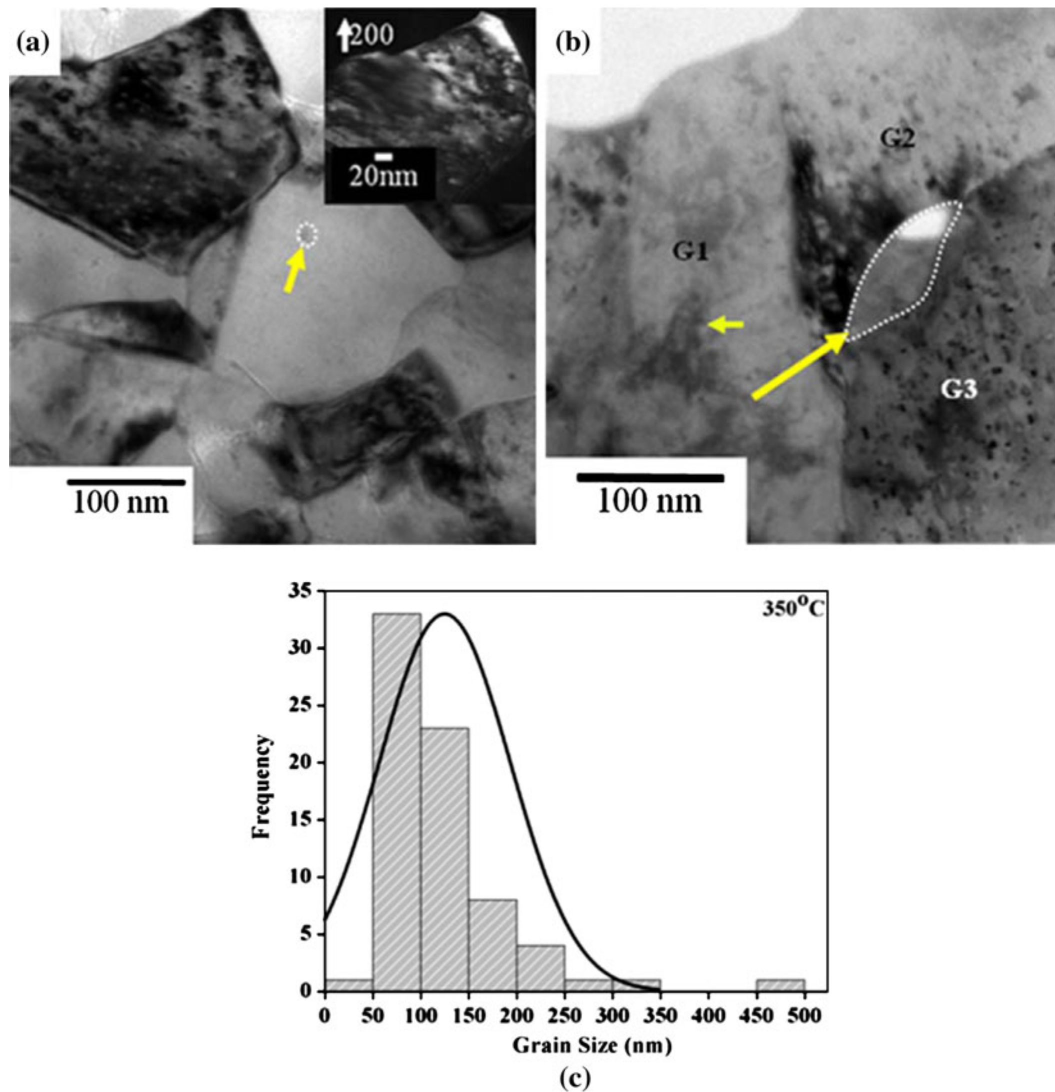

Fig. 7—(*a*) Bright-field micrograph of Cu-10 wt pct Pb sample processed at sintering temperature of 623 K (350 °C) and 100 MPa. (*b*) Bright-field micrograph showing encapsulated Pb at nanocrystalline Cu grain boundary. (*c*) Cu grain-size distribution. The inset in (a) shows a dark-field micrograph revealing deformation structure. Arrows mark the Pb position in the matrix.

for samples sintered at lower temperatures of 573 K to 673 K (300 °C to 400 °C). The possible reasons for significant enhancement of densification by incorporation of second phase (Pb) and microstructural evolution will be discussed in this section in reference to the following aspects:

(a) solid-state sintering of the Cu matrix,
(b) LPS of the Cu-10 wt pct Pb alloy,
(c) grain growth of the matrix, and
(d) morphology of Pb in the microstructure.

(a) It is widely recognized that a major difficulty in synthesis of nanostructured materials is the grain growth during sintering.[12] The use of "activated" sintering, involving a combination of lower temperature and shorter time, makes it possible to obtain a bulk nanocomposite; in particular, the advent of field assisted sintering techniques, *e.g.*, SPS has the advantage in fabrication of bulk nanocomposite, such as Cu-Pb.[13] As indicated earlier, SPS involves the application of pulsed electrical direct current in combination with resistance heating to achieve a high heating rate, so that grain coarsening can be minimized. Because of the high heating rate, the final sintering temperatures can be reached in less time. This has the advantageous implication of suppressing the low-temperature densifying mechanism (such as surface diffusion); hence, grain coarsening/growth can be contained within the nanocrystalline regime. The observation of nanocrystalline Cu grains in the Cu-10 wt pct Pb alloy, therefore, is consistent with the inherent advantage of SPS in the narrow temperature window of 573 K to 673 K (300 °C to 400 °C). However, significant grain growth during SPS takes place in the Cu-10 wt pct Pb alloy at $T > 673$ K (400 °C). The sintering mechanisms in the present case can be explained from the point of view of

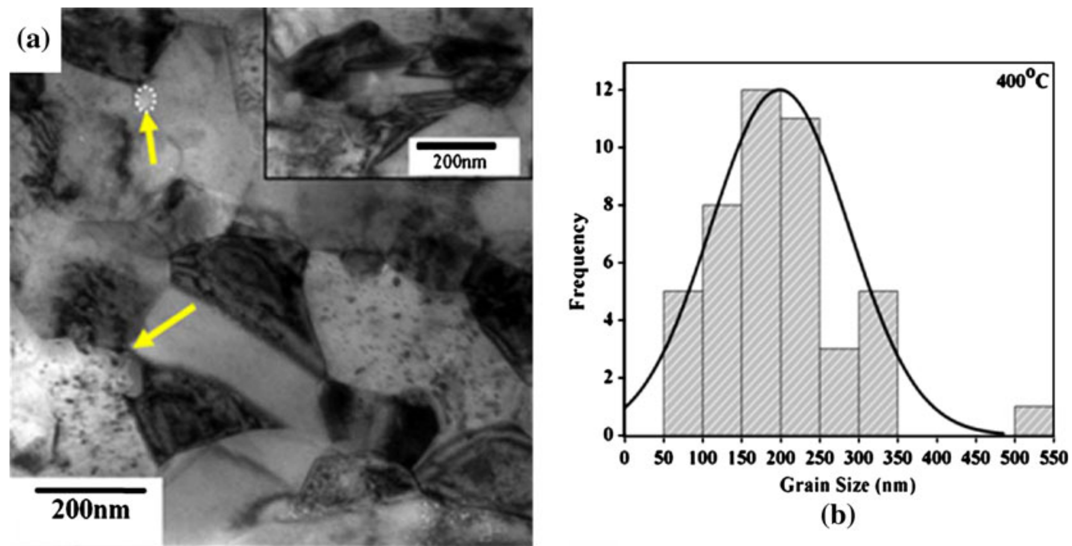

Fig. 8—(*a*) Bright-field micrograph of Cu-10 wt pct Pb sample processed at sintering temperature of 673 K (400 °C) and 100 MPa. (*b*) Cu grain-size distribution. The inset in (a) shows elongated grain morphology of nanocrystalline Cu grains. Arrows mark the Pb position in the matrix.

microstructure development. It is known that nanocrystalline particles have a significant volume fraction of interfaces, such as grain boundaries, which provide faster diffusion paths for mass transport. Also, a significant number of contacting points are available in a powder compact of nanocrystalline powders; therefore, pulsed direct current flow experiences more resistance at such multiple contact points at particles boundaries. The application of electrical current will further mobilize the sintering process.

The effect of electric current on sintering depends on the electrical conductivity of powder particles. A thin layer of oxide film on nanocrystalline Cu particles is expected to form during heating to the sintering temperature. The copper oxide has much higher resistivity ($\rho_{\mathrm{CuO}} \sim 20\ \Omega\mathrm{m}$)[14] as compared to highly conducting copper ($\rho_{\mathrm{Cu}} \sim 1.58 \times 10^{-8}\ \Omega\ \mathrm{m}$).[15] At the initial stage of sintering, the electric field produces electrical discharges between the surface oxide film and possibly plasma in the interparticle void space. The surface oxide film of the Cu particles is then removed because of the voltage breakdown effect followed by removal of absorbed gases from the powder in vacuum. This leads to the surface activation of Cu powder particles. From the preceding, it can be stated that spark discharges due to multiple contact resistance at activated Cu-Cu, Cu-Pb, or a few Pb-Pb interfaces would increase the localized temperature at the neck region. For Cu-Cu contacts, this causes a concomitant increase in solid-state diffusivity of Cu atoms. This also leads to faster neck growth at Cu-Cu contacts. Once a neck forms between the two particles, the heating due to the sparking effect will be replaced by heating of the neck and particle by conventional Joule heating, which is proportional to the square of current. The conduction of electrical current through an assembly of powder particles is found to be controlled by a parameter known as "constriction resistance" (R_c):[16]

$$R_c(n, a, l) = \frac{\rho f_s}{2\pi n a} \arctan\left(\frac{\sqrt{l^2 - a^2}}{a}\right) \qquad [3]$$

where a is the linear dimension of the interparticle contact, ρ is the resistivity of the powder, l is the nearest distance between contacts, and f_s is a shape factor. A higher R_c value is expected for nanocrystalline Cu particles; since R_c is inversely proportional to the linear dimension of the interparticle contact, a localized region of high resistance is formed at interparticle contacts. The application of electric current, therefore, will lead to high Joule heating and, therefore, a sharp increase in local temperatures. The bulk sample will be densified quickly because of the rapid increase in temperature. The retention of the finer crystallite size of Cu matrix will also cause an enhancement of sintering kinetics due to augmentation of the sintering driving force. According to Herring's scaling law,[17] the sintering time follows a direct power law relationship with particle size. The finer the particles size, the faster will be the grain boundary diffusion induced mass transport to neck region. Therefore, the retention of nanograins essentially reflects the GB diffusion dominated neck growth kinetics during SPS at $T \leq 673$ K (400 °C).

The additional contribution to enhanced mass transport can be ascribed to short circuit diffusion, enhanced due to the presence of a large number of line defects, *i.e.*, dislocation network (Figure 7(a)). The dislocations and twin boundaries are generated in Cu grains due to plastic deformation during SPS. The localized temperature increase, as discussed previously, can aid in deformation of Cu under external pressure of 100 MPa during our SPS experiments. Summarizing, the retention of finer particle size, *i.e.*, faster GB diffusion at interparticle neck region and short circuit diffusion *via* dislocations, can explain the faster solid-state sintering of Cu during SPS, in the temperature region of $T/T_m < 0.5$.

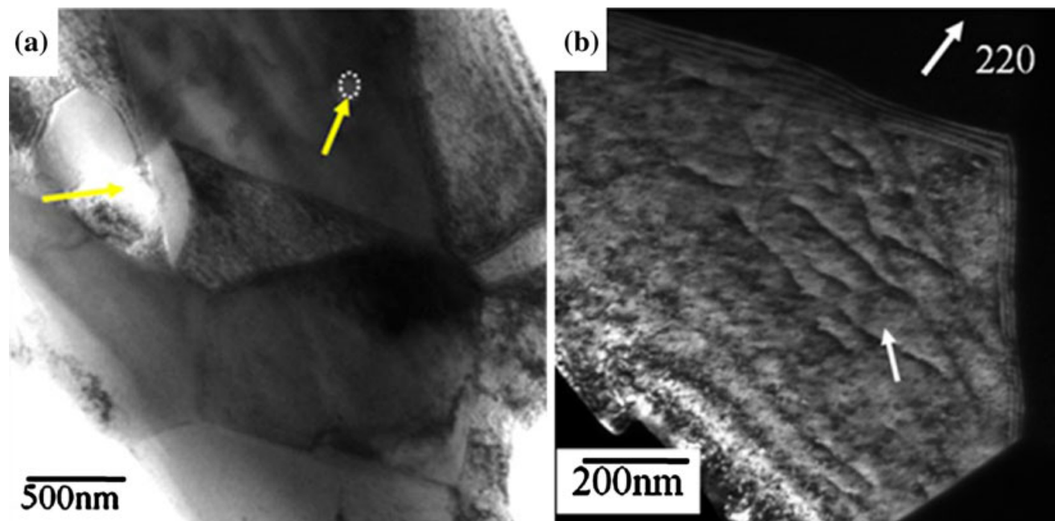

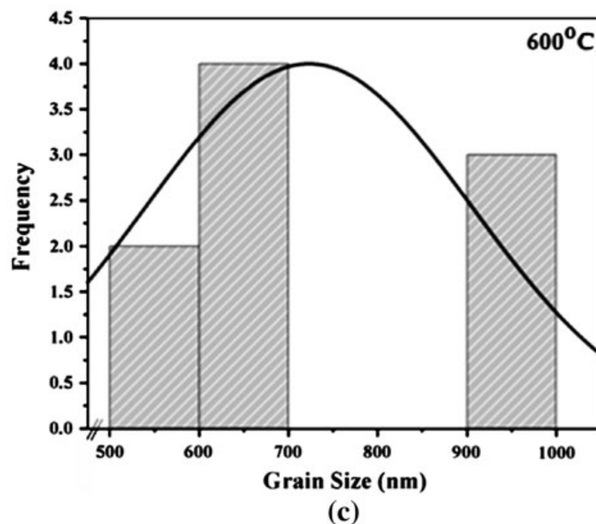

Fig. 9—(*a*) Bright-field micrograph of Cu-10 wt pct Pb sample processed at sintering temperature of 873 K (600 °C) and 100 MPa. (*b*) Single grown Cu grain depicting a lot of dislocation activity inside it. (*c*) Cu grain-size distribution. In (a), the arrow shows the entrapped Pb-particle inside Cu grains. In (b), the white arrow inside the grain shows dislocations.

(b) In the case of the Cu-10 wt pct Pb alloy, the Pb particles are skin molten at 573 K (300 °C) (Figure 5(a)). Therefore, the densification is aided by the presence of skin melted Pb particles leading to faster diffusion of atoms to neck regions. However, as the temperature is increased to 623 K (350 °C), *i.e.*, greater than the equilibrium melting temperature of Pb, LPS additionally contributes to enhanced densification. At this temperature, fully molten Pb-rich liquid thus formed around the Cu grains would promote a faster diffusion path, leading to rapid densification. Although Pb has inferior electrical conductivity ($\rho_{Pb} \sim 19.3 \times 10^{-8}\ \Omega$ m)[14] compared to Cu, a large fraction of current will still flow through the powder compact as the amount of Pb is only 10 wt pct. Therefore, Joule's heating induced melting of Pb will lead to LPS of the Cu-10 wt pct Pb compact. The dilatometer studies of the green compact of nanocrystalline Cu-10 wt pct Pb from RT to 873 K (600 °C) show appreciable dimensional shrinkage after the Pb melting point has been exceeded (Figure 11(b)). This is a reflection of the enhanced mass transport phenomenon. More information on heating induced shrinkage behavior of Cu and Cu-10 wt pct Pb green compact can be analyzed on the basis of dilatometry data, presented in Figure 11. In the case of pure Cu, the shrinkage starts around 348 K (75 °C) and continues until 419 K (146 °C) (Figure 11(a)). This can be attributed to the reduction of cuprous oxide Cu_2O in the ambient atmosphere during the course of heating in the dilatometer:

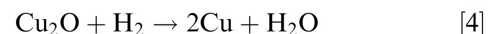

$$Cu_2O + H_2 \rightarrow 2Cu + H_2O \quad [4]$$

The water vapor, thus formed above 373 K (100 °C), will then be removed in the course of pressureless dilatometry, leading to shrinkage. The observation of a plateau in the temperature range of 419 K to 562 K (146 °C to 289 °C) in the case of pure Cu indicates any lack of densification and possibly surface diffusion taking place in this region, which does not contribute

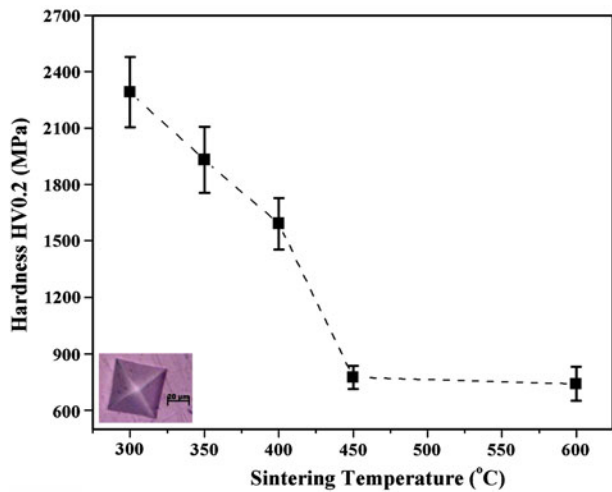

Fig. 10—Hardness measurement of nanocrystalline Cu-10 wt pct Pb, SPS at 100 MPa.

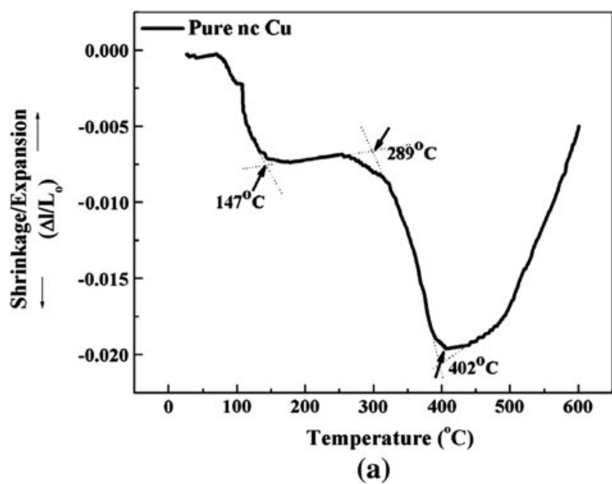

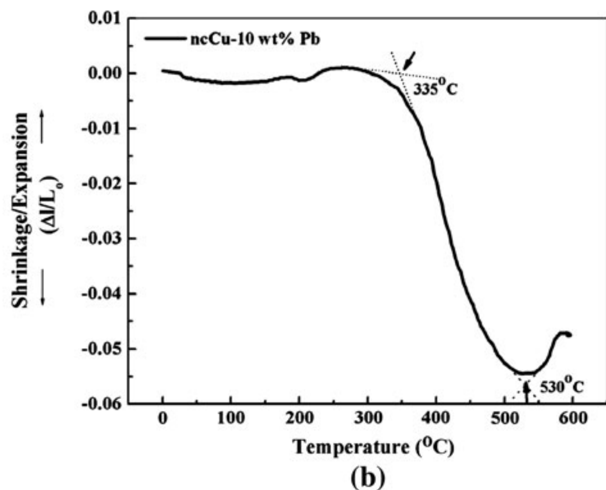

Fig. 11—Dilatometer plots obtained at a heating rate of 5 K/min with the green compacts of (*a*) pure nanocrystalline Cu and (*b*) nanocrystalline Cu-10 wt pct Pb.

to overall shrinkage (Figure 11(a)). The continuous shrinkage in the temperature range of 562 K to 675 K (289 °C to 402 °C) in the case of pure Cu essentially reflects continuous neck growth by solid-state grain boundary diffusion. The maximum shrinkage that occurs around 675 K (402 °C) in pressureless dilatometry corresponds closely to 673 K (400 °C), the temperature of maximum density in the case of SPS of pure Cu. However, the heating above 679 K (406 °C) leads to clear expansion of the compact, and this is the region (Figure 2) where density decreases.

For the case of Cu-10 wt pct Pb compact, the pressureless dilatometry exhibits no significant change until 608 K (335 °C) (Figure 11(b)). There is no perceptible shrinkage or expansion until 608 K (335 °C) for Cu-10 wt pct Pb. Beyond 608 K (335 °C) (>600 K (327 °C), melting temperature of Pb), the Pb particles melt and, thereafter, a continuous shrinkage in the presence of liquid phase occurs up to 803 K (530 °C).

As far as SPS of Cu-10 wt pct Pb is concerned, relative density values from 523 K to 623 K (250 °C to 350 °C) show a steep increase (Figure 2). The maximum in density is obtained at 623 K (350 °C) (>600 K (327 °C), melting temperature of Pb) as opposed to 803 K (530 °C) in pressureless dilatometry. It should be mentioned here that pressureless dilatometry does not simulate SPS processing, which involves simultaneous application of pressure and high electrical current. Therefore, this can be explained by considering the simultaneous application of pressure of 100 MPa and electric current during SPS processing. While, on one hand, the softer Pb particles are more susceptible toward pressure, on the other hand, the favorable electrical conductivity of Cu particles will be responsible for mobilizing the densification process by bypassing the electric current through their bulk.

Beyond 673 K (400 °C), the wetting behavior of molten Pb on Cu particles and grain-growth kinetics of Cu play a significant role in determining the densification kinetics. The dewetting of Cu grains by molten Pb (as evident from Figures 5(c) and (d)) and the abnormal increase of mean grain size of Cu beyond 803 K (530 °C) (Figure 11(b)) will lead to a sharp decrease in relative density of Cu-10 wt pct Pb as compared to pure Cu, during SPS (note the slopes beyond the maximum densities for pure Cu and Cu-10 wt pct Pb in Figure 2). It has been reported in the literature that the interfacial energy between liquid Pb and solid Cu ($\gamma_{\mathrm{Pb}(l)/\mathrm{Cu}(s)}$) is temperature dependent.[18] According to Empl *et al.*, the liquid Pb does not wet Cu grains beyond 673 K (400 °C). Although, liquid Pb is present in the sample, it leads to a decrease in densification due to dewetting of Cu grains. The Pb particles are found to be exuded out of the Cu-10 wt pct Pb compact when sintered at the temperature of 873 K (600 °C). This temperature-dependent wetting explained well our observations of decrease in density in the temperature range of 723 K to 873 K (450 °C to 600 °C) (Figure 2).

Since LPS involves the liquid formation at interparticle pores as well as wetting of the liquid phase at the GB region, an estimation of the porosity as well as consideration of the wetting angle or amount of liquid formation is important. The measured green density of Cu-10 wt pct Pb compact has been found to be 41.4 pct of ρ_{th}. Therefore, 58.6 pct pore space is present in the

green compact. Figure 12 shows pore-size distribution in the green compact obtained by Brunauer, Emmett, Teller (BET) measurement. The measurement indicates that the maximum pore size is about 100 nm, with the predominant size being 60 nm. As the liquid phase forms at the sintering temperature of 623 K (350 °C) (Figure 11(b)), the liquid Pb flows into these fine capillaries due to the capillary pressure difference between the solid Cu particles. The solid Cu grains are surrounded by liquid Pb, which provides both capillary force and transport medium. The grain rearrangement occurs in response to the capillary force, causing uniform densification and contact flattening between the grains. The capillary force pulling the Cu particles toward each other is responsible for the initial densification by rearrangement of Cu particles. This force in the liquid-Pb film is affected by the geometrical parameters: liquid volume fraction f_l, particle radius s, interparticle distance l, neck radius x, interfacial energy γ_l, and wetting angle of copper particles by lead φ:[19]

$$F = \gamma_l \left[\pi s^2 \sin^2 \psi \left(\frac{1}{r} - \frac{1}{x} \right) + 2\pi s \sin \psi \sin(\pi + \varphi) \right] \quad [5]$$

The grain boundary wetting of Cu by Pb is quantified by the dihedral angle, φ, subtended by the liquid Pb along the solid/solid/liquid triple line. Empl *et al.*[17] showed that the mean value of φ remains nearly constant over a wide range of temperature before dropping to zero above 1173 K (900 °C) for Cu-1 wt pct Pb alloy. The reported mean value of φ is about 60 deg at 1173 K (900 °C). In the present case, the wetting angle may be larger as the compact is being densified at a much lower temperature of 623 K to 673 K (350 °C to 400 °C). However, the amount of liquid Pb will be more than that reported by Empl *et al.*[17] The amount of liquid formed at a particular sintering temperature is determined by the lever rule. The Cu-Pb equilibrium phase diagram data were used here to calculate the weight percent of liquid forming at different sintering temperatures. Figure 13 shows the results of such calculation. One can clearly observe that the weight percent of liquid remains constant (~10 wt pct) at all sintering temperatures except at 573 K (300 °C). Since the capillarity pressure varies directly as the reversal of the particle size, capillary pressure would be very high to cause particle rearrangement and sliding for nanosized Cu particles. This leads to attainment of high sinter density for samples sintered at temperatures of 623 K to 673 K (350 °C to 400 °C) due to high capillarity pressure.

(c) The TEM results indicate the matrix Cu grains undergo extensive growth when sintered at 723 K to 873 K (450 °C to 600 °C) (Figures 6 through 9). The average grain size for the sample sintered at 873 K (600 °C) is 723 ± 183 nm, which is almost two orders of magnitude higher than the initial grain size of Cu powder 97 ± 25 nm. Horvath *et al.* reported remarkable resistance to grain growth of Cu, when heated to 498 K (225 °C).[20] A detailed study carried out by Ganapathy *et al.*[21] indicates that nanocrystalline Cu does undergo extensive grain growth when heated to 673 K (400 °C). Our results also suggest similar grain growth characteristics at a sintering temperature of above 673 K (400 °C). Due to the high heating rates used in SPS, the time available for nanocrystalline Cu grain growth is small as compared to other studies. It is well known in the literature that pores hinder grain growth during sintering.[22] The density measurement reveals 10 to 12 pct porosity in green compacts (Figure 2). Therefore, a high heating rate and the presence of pores are responsible for Cu grains not growing extensively even at a sintering temperature of 673 K (400 °C). A careful look at the histogram of the sample sintered at 873 K (600 °C) (Figure 9(b)) shows that Cu grains undergo abnormal grain growth. There are few grains with size of 1 μm, whereas a large number of grains have sizes in the range of 0.5 to 0.7 μm. A plausible explanation is that enhanced GB mobility for some of the grains preferentially oriented along the electric field direction during SPS can lead to abnormal

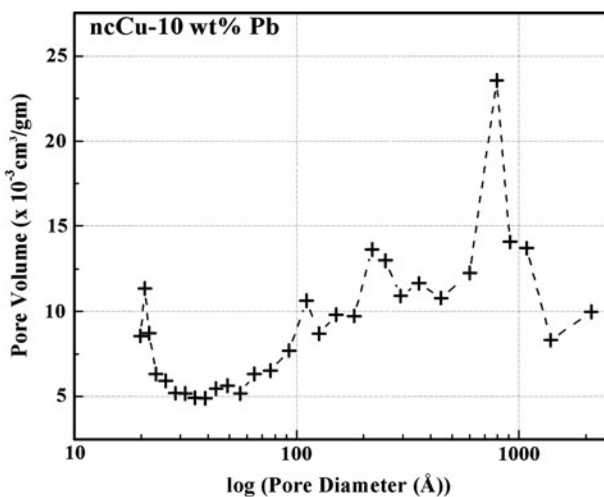

Fig. 12—Pore-size distribution of the nanocrystalline Cu-10 wt pct Pb green compact.

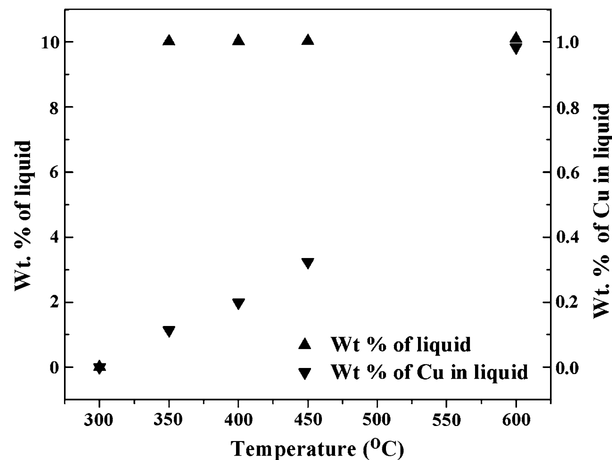

Fig. 13—Estimation of weight percent of liquid at different sintering temperatures and weight percent of Cu dissolved in liquid. The estimation was done using a Cu-Pb equilibrium phase diagram, shown in Fig. 1.

grain growth. Another explanation can be put forward based on the literature report. It is reported that the onset of abnormal grain growth occurs when the ratio of the largest grain size to the average size is $d_{\max}/d_{av} > 2$.[23] In the present case, this ratio is found to be 1.7 (1/0.6), which is lower than the reported value. It should be noted that grain size measurements have been done using images obtained by TEM, which allows us to observe a small volume of the sample. However, the scanning electron microscope images show that $d_{av} \sim 0.4$ μm and, therefore, $d_{\max}/d_{av} = 2$.[22] This can explain the abnormal grain growth of Cu grains during SPS at 873 K (600 °C).

(d) The detailed microscopic observations show different shapes and sizes of the second phase (Pb) in the sintered microstructure. This can be explained using the Cu-Pb phase diagram (Figure 1) and pore size distribution in the green compact (Figure 12). Keeping in mind the three orders of size difference of constituent powder particles, Cu being nanocrystalline and Pb microcrystalline, the pore size distribution will have an important role to play in deciding the morphology of Pb. The pore-size distribution for the green compact of Cu-10 wt pct Pb reveals the maximum pore diameter to be around ~ 0.21 μm (Figure 12). Therefore, the presence of the Pb particles having size range 1 to 2 μm is definitely not due to resolidification of Pb particles inside the pores.

Figure 1 shows the binary Cu-Pb equilibrium phase diagram.[8] The Pb is barely soluble in Cu, and Cu has limited solubility in Pb. Figure 13 plots the estimated solubility of Cu in liquid Pb as a function of temperature. Such estimation has been carried out on the basis of the equilibrium phase diagram, as shown in Figure 1. It can be observed that only 0.4 wt pct Cu is soluble in liquid Pb at 723 K (450 °C), whereas about 1 wt pct Cu is soluble in liquid Pb at 873 K (600 °C). It should be noted here that the solubility of Cu in liquid Pb would be higher than that estimated using the equilibrium phase diagram. This is attributed to three factors: (1) nonequilibrium nature of the processing, (2) nanosized Cu grains, and (3) application of large external pressure (100 MPa).

During SPS at 573 K (300 °C), which is below the eutectic temperature, the Pb particles at Cu grain boundaries do not undergo melting and remain as agglomerated solid particles sitting along Cu grain boundaries. The solid particles deform due to application of high pressure during sintering (inset of Figure 5(a)).

However, sintering at 623 K (350 °C) and higher temperature leads to melting of the Pb particles at the grain boundaries of Cu. The molten Pb easily flows through the Cu grains forming a flowlike pattern in the microstructure (Figures 5(b) and (c)). A small amount of Cu (~0.1 wt pct at 623 K (350 °C)) is dissolved in liquid Pb, which, during cooling, forms discrete particles of Pb within the Cu grains as well as grain boundaries (Figures 7(a) and (b)). The binary Cu-Pb phase diagram also indicates that Pb-rich liquid, containing a very small amount of Cu, undergoes a eutectic reaction at ~599 K (326 °C), leading to formation of discrete Pb inclusions in the Cu matrix. This additional Cu, which is disposed out of the liquid, will surround the Pb particles, subsequently entrapping them within its bulk. However, still most of the inclusions are located at the grain boundaries (Figures 6(a) and 7(b)) or at grain boundary triple pockets (Figure 7(a)).

Beyond 673 K (400 °C), it was found from TEM analysis that the grain size distribution of Cu shifts to higher values because of the abnormal grain growth. In the course of the growth process, the Pb particles, specifically located at the grain boundary regions of Cu grains, will be entrapped by the growing Cu grains.

At 873 K (600 °C), the molten Pb-rich liquid in contact with Cu grains, during the cooling cycle of SPS, undergoes the eutectic reaction and forms discrete Pb particles, which rapidly develop equilibrium shape by diffusion of Cu through the molten Pb (Figure 5(d)). The morphology of the Pb particles in the Cu matrix can be explained by considering the variation in interfacial energy. It has been reported in the literature that the interfacial energy of Pb(liquid)/Cu(solid) ($\gamma_{\mathrm{Pb}(l)/\mathrm{Cu}(s)}$) is temperature dependent.[17] These authors have mentioned that beyond 723 K (450 °C), Pb does not wet the Cu grains and will act more readily to changes in interfacial energy and will therefore assume the geometrically isotropic shape of a sphere. After sintering at 873 K (600 °C), the Pb particles (located well inside the compact) were found to form the spherical discrete inclusions inside the Cu grains (Figure 5(d)). Also, some of the Pb particles (located in the vicinity of the compact surface) were exuded out of the compact due to dewetting of the Cu grains by Pb.

V. CONCLUSIONS

The present work has demonstrated that it is possible to obtain nearly dense Cu-10 wt pct Pb nanostructured alloy by tailoring SPS conditions. In particular, the following major conclusions can be drawn.

1. Around 90 pct ρ_{th} is attained in nanocrystalline Cu at 673 K (400 °C) and in Cu-10 wt pct Pb at 623 K (350 °C) during SPS in argon atmosphere at 100 MPa pressure.
2. A transition from nanocrystalline microstructure to micron-sized grain morphology occurs in Cu-10 wt pct Pb compact during SPS in the temperature range of 723 K to 873 K (450 °C to 600 °C).
3. The enhanced densification of Cu-10 wt pct Pb at lower temperature has been explained in terms of LPS assisted by wetting of molten Pb liquid.
4. A high hardness of around 2 GPa has been measured in Cu-10 wt pct Pb alloy after SPS at a temperature of 573 K (300 °C). The grain growth at higher temperature leads to lowering of hardness.
5. Both the lenticular shaped Pb at grain boundary regions of Cu grains and spherical shaped Pb within Cu grains are some of the important characteristics of nanostructured Cu-10 wt pct Pb alloy.

REFERENCES

1. S. Anand, T.S. Srivatsan, and T.S. Sudarshan: *J. Mater. Sci.*, 1993, vol. 28, pp. 4615–22.
2. T.S. Srivatsan and T.S. Sudarshan: *J. Mater. Sci. Lett.*, 1995, vol. 14, pp. 864–68.
3. V.E. Buchanan, P.A. Molian, T.S. Sudarshan, and A. Akers: *Wear*, 1991, vol. 146, pp. 241–56.
4. Priyanka Dash: M. Tech Dissertation, Indian Institute of Technology, Kanpur, 2006.
5. J.R. Groza: *Nanostruct. Mater.*, 1999, vol. 12, pp. 987–92.
6. B. Günther, A. Kumpmann, and H.D. Kunze: *Scripta Metall. Mater.*, 1992, vol. 27, pp. 833–38.
7. S.W. Wang, L.D. Chen, Y.S. Kang, M. Niino, and T. Hirai: *Mater. Res. Bull.*, 2000, vol. 35, pp. 619–28.
8. D.J. Chakrabarti and D.E. Laughlin: *Binary Alloy Phase Diagrams*, T.B. Massalski, J.L. Murray, and L.H. Bennett, eds., ASM International, OH, 1986, vol. I.
9. N.K. Mukhopadhyay and P. Paufler: *Int. Mater. Rev.*, 2006, vol. 51, pp. 209–45.
10. T.S. Srivatsan, B.G. Ravi, A.S. Naruka, L. Riester, S. Yoo, and T.S. Sudarshan: *Mater. Sci. Eng. A*, 2001, vol. 311, pp. 22–27.
11. Z.H. Zhang, F.C. Wang, L. Wang, S.K. Li, M.W. Shen, and S. Osamu: *Mater. Charact.*, 2008, vol. 59, pp. 329–33.
12. A. Mukhopadhyay and B. Basu: *Int. Mater. Rev.*, 2007, vol. 52, pp. 1–32.
13. Z.A. Munir, U.A. Tamburini, and M. Ohyanagi: *J. Mater. Sci.*, 2006, vol. 41, pp. 763–77.
14. M.T.S. Nair, L. Guerrero, O.L. Arenas, and P.K. Nair: *Appl. Surf. Sci.*, 1999, vol. 150, pp. 143–51.
15. *Smithells Metals Reference Book*, 7th ed., E.A. Brandes and G.B. Brook, eds., Butterworth-Heinemann, Great Britain, pp. 19-1–19-2.
16. R. Holm: *Electric Contacts: Theory and Application*, 4th ed., Springer-Verlag, New York, NY, 1967.
17. C. Herring: *J. Appl. Phys.*, 1950, vol. 21, pp. 301–03.
18. D. Empl, L. Felberbaum, V. Laporte, D. Chatain, and A. Mortensen: *Acta Mater.*, 2009, vol. 57, pp. 2527–37.
19. V.N. Eremenko, Y.V. Naidich, and I.A Lavrinenko: *Liquid Phase Sintering*, Consultants Bureau, New York, NY, 1970.
20. J. Horváth, R. Birringer, and H. Gleiter: *Solid State Commun.*, 1987, vol. 62, pp. 319–22.
21. S.K. Ganapathy, D.M. Owen, and A.H. Chokshi: *Scripta Metall. Mater.*, 1991, vol. 25, pp. 2699–704.
22. W.D. Kingery, H.K. Bowen, and D.R Uhlmann: *Introduction to Ceramics*, Wiley, New York, NY, 1976.
23. M. Hillert: *Acta Metall.*, 1965, vol. 13, pp. 227–38.